Electronic Supplementary Information （ESI）

A Novel Photochemical Vapor Generation Medium: Diketone as Medium for Determination of Tellurium and Bismuth by ICP-MS

Yuqi Li[a], Lu Zhang[a], Hanjiao Chen[*b], Yuanming Zhai[*b], Xiandeng Hou[abc]

[a]*College of Chemistry, Sichuan University, Chengdu, Sichuan 610064, China.*

[b]*Analytical & Testing Centre, Sichuan University, Chengdu, Sichuan 610064, China. Email: hanjiao.chen@scu.edu.cn*

[c]*National and Local Joint Engineering Laboratory for Energy Plant Bio-oil Production and Application, Key Laboratory of Green Chemistry and Technology (Ministry of Education), Sichuan University, Chengdu, Sichuan 610064, China.*

*Corresponding Authors' E-mail: hanjiao.chen@scu.edu.cn;

yuanmingzhai@scu.edu.cn.

EXPERIMENTAL SECTION

Instrumentation.

An iCAP Q inductively coupled plasma mass spectrometer (Thermo Fisher Scientific Inc., Germany) was used for detection of ^{130}Te and ^{209}Bi throughout this work. A PVG-system (Leishan Optoelectronic Technology Co., Ltd., Nanking, China) which provides 185 and 254 nm UV irradiation was constructed to replace the nebulizer and spray chamber for determination (Fig. S1). An X-band electron paramagnetic resonance (EPR) spectrometer (EMX plus, Bruker, Germany) was used for identification of radicals during PVG with 5,5-dimethyl-1-pyrroline N-oxide (DMPO) as a spin trap. Simulation of the EPR spectra was accomplished using EasySpin in Matlab.

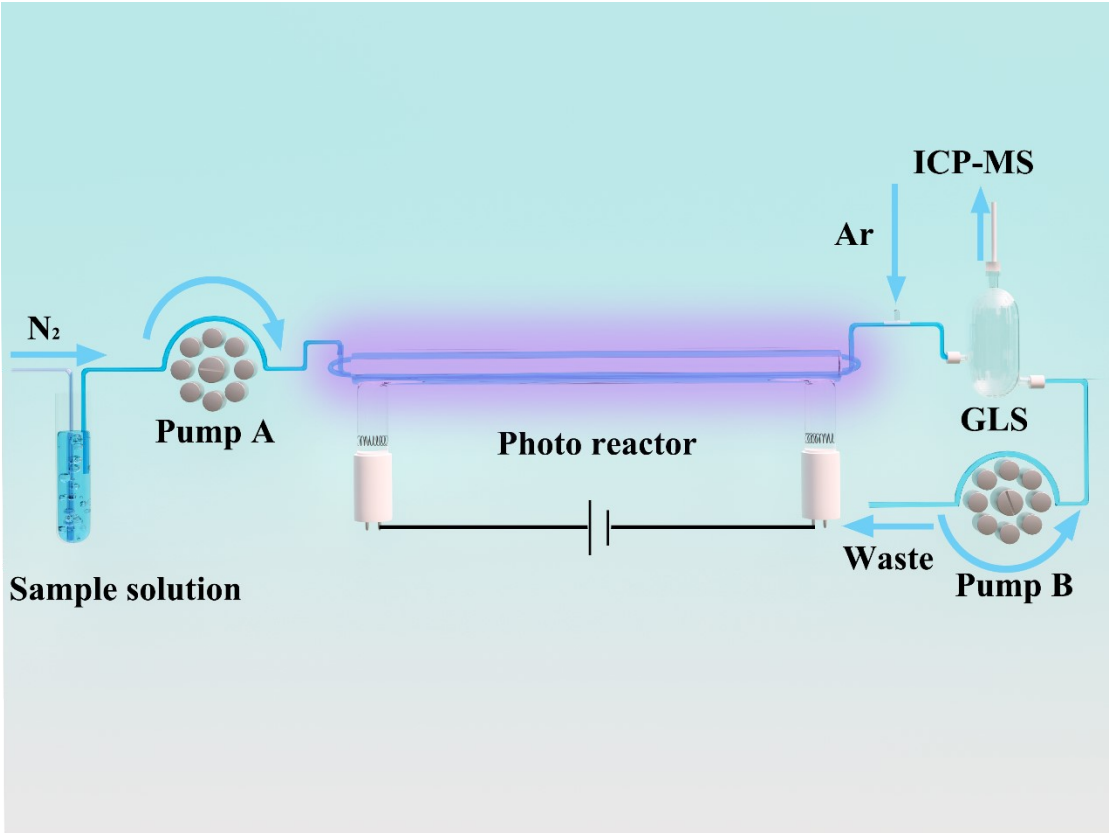

Fig. S1. Schematic illustration of the PVG inlet system.

Reagents and Materials.

All reagents used in this study were of at least analytical grade. Ultrapure Water (18.2 MΩ cm) obtained from a Milli-Q water system (Chengdu Ultrapure Technology Co., Ltd., Chengdu, China) was used to prepare the solutions. Acetylacetone and butanedione were sourced from Chron Chemicals (Chengdu, China) and Macklin Biochemical Co., Ltd. (Shanghai, China) respectively. Certified standard stock solutions of Te (1000 mg/L) and Bi (1000 mg /L) were acquired from Century Aoke

Biotechnology Co., Ltd. (Beijing, China). $Co(CH_3COO)_2 \cdot 4H_2O$ and $Fe(CH_3COO)_2$ were obtained from Aladdin Reagent Co. (Shanghai, China) and used to prepare stock solutions (1000 mg/L). DMPO was purchased from Dojindo Laboratories (Shanghai, China). The accuracy of the proposed method was further studied on natural mineral water samples from 2 different brands and lake sample based on spike recovery tests.

Analytical Procedure.

Prior to analysis, all sample solutions were purged with high-purity nitrogen gas (≥99.999%) for a minimum of 20 minutes to effectively reduce dissolved oxygen (DO). Following this, samples were delivered to the PVG reactor using a peristaltic pump operating at 6.80 mL/min. The pump was then stopped to allow the samples to remain in the photoreactor for optimized durations: 120 s for Te reduction and 150 s for Bi reduction. Subsequently, the irradiated sample was transferred to the GLSs at the same sample flow rate for analyzing by ICP-MS. The peak area of the ^{130}Te and ^{209}Bi isotope were used to construct an external calibration curve for samples.

NMR Characterization.

All the ^{1}H and ^{13}C NMR experiments were performed on a Bruker Avance III 800 MHz spectrometer (Bruker, Switzerland) operating at 800.13 MHz for ^{1}H frequency and 201.19 MHz for ^{13}C frequency, respectively, equipped with a 5 mm $^{1}H/^{13}C/^{15}N/^{31}P$ cryo-probe. The chemical shifts for both ^{1}H and ^{13}C were calibrated with reference to the signals observed for TMS.

TEM and EDS Characterization.

As for the gas-phase products. The reaction solution, prepared at selected experimental concentrations, was irradiated in the PVG reactor. The product mixture was transferred to the gas-liquid separator. After sealing the drain port to direct flow through the upper vent, a carrier gas stream (200 mL/min) was initiated. The gas-phase products were collected on a copper mesh placed over the vent for 10 min, after which the mesh was dried under a lamp.

As for the liquid-phase products. A 10 μL liquid product was applied onto the surface of the copper mesh, which was subsequently dried under a lamp. Based on the measurement results, the solution volume could be increased or decreased. TEM and EDS characterizations are the same samples.

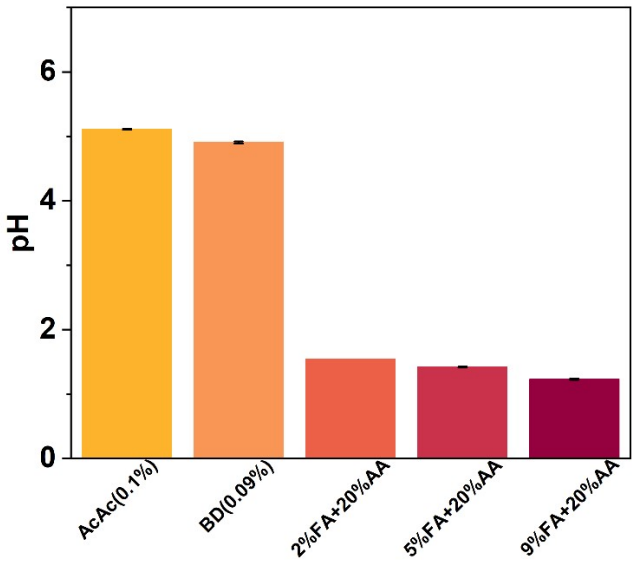

Fig. S2. The comparison of pH values under optimal testing conditions in different media

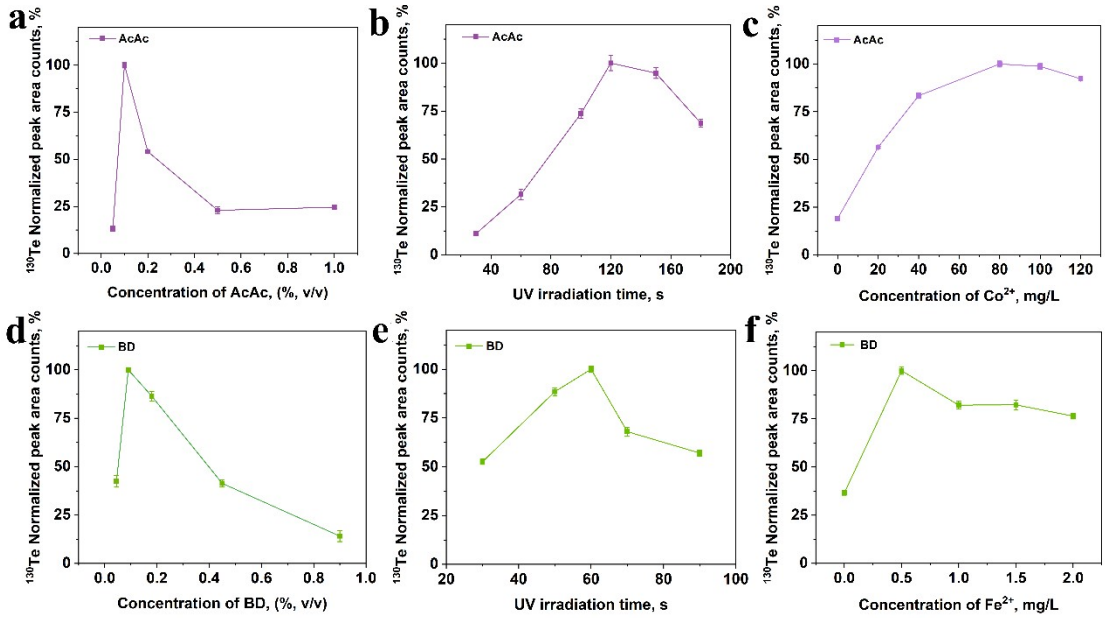

Fig. S3. A concentration of 10 μg/L Te was used in all the following experiments. (a) the media concentration optimization for ^{130}Te in AcAc medium; (b) the UV irradiation time optimization for ^{130}Te in AcAc medium (0.1%, v/v); (c) the homogeneous sensitizers concentration optimization for ^{130}Te in AcAc medium (0.1%, v/v), UV irradiation time: 120 s; (d) the media concentration optimization for ^{130}Te in BD medium; (e) the UV irradiation time optimization for ^{130}Te in BD medium (0.09%, v/v); (f) the homogeneous sensitizers concentration optimization for ^{130}Te in BD medium (0.09%, v/v), UV irradiation time: 60 s;

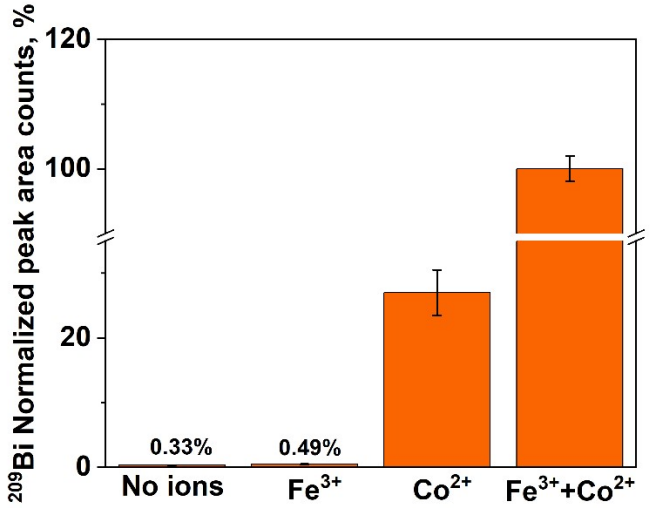

Fig. S4. The synergistic effect from Fe^{3+} and Co^{2+}. Test condition: Bi (5 μg/L); AcAc (0.05%, v/v); Fe^{3+} (7 mg/L); Co^{2+}(90 mg/L); UV irradiation time: 150 s.

As shown in Fig. S4, Fe^{3+} could enhance the peak area in a slight way, with a slightly rose from 0.33% to 0.49%. Although Co^{2+} could significantly enlarge the peak area from 0.33% to 27%, it was weaker than the synergistic effect from Fe^{3+} and Co^{2+}. Through the synergistic effect from Fe^{3+} and Co^{2+}, the peak area of ^{209}Bi increased by a factor of 300 compared to without metal ions. In other words, the combined effect of Fe^{3+} and Co^{2+} that is greater than the cumulative effect that those sensitizers produced when used individually, which is a symbol of synergistic effect.[1]

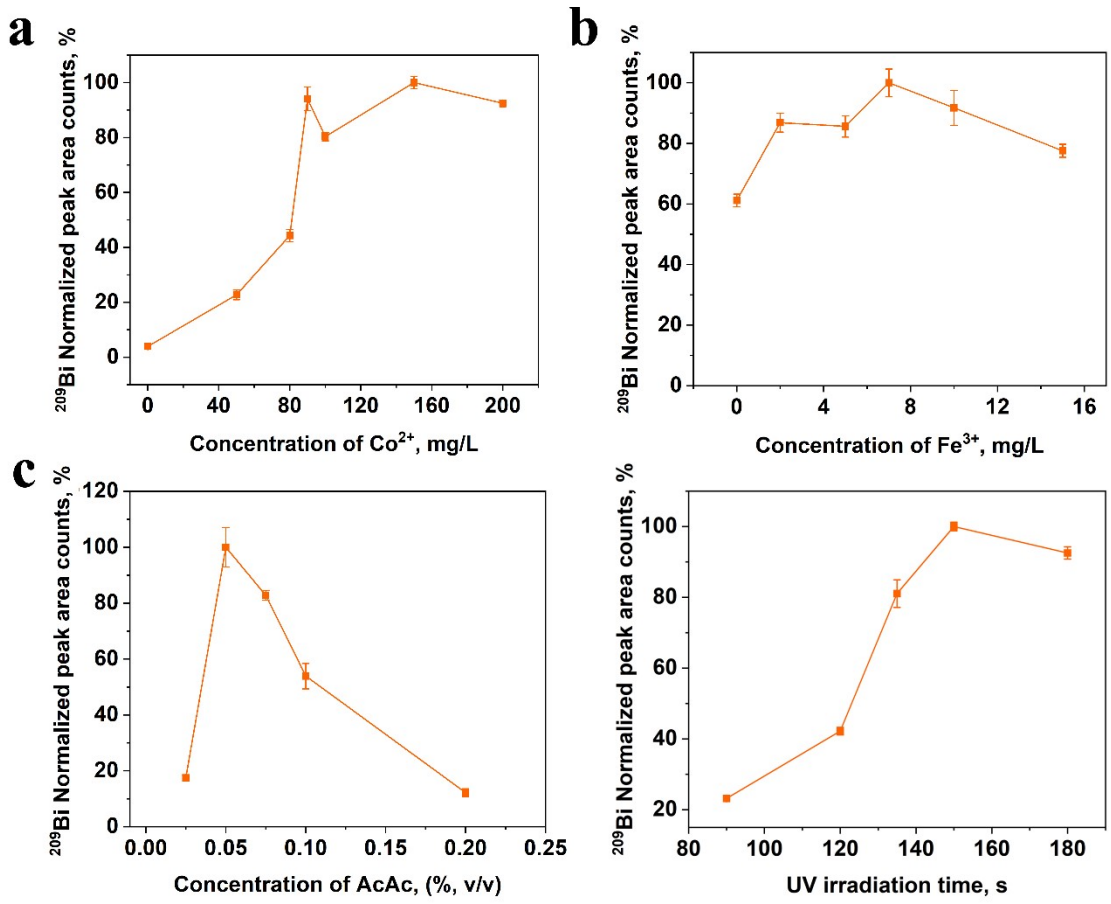

Fig. S5. A concentration of 0.1 μg/L Bi was used in the following experiments. (a) the homogeneous sensitizers concentration optimization for ^{209}Bi in AcAc medium (0.1%, v/v), UV irradiation time: 120 s, Fe^{3+} (10 mg/L); (b) the homogeneous sensitizers concentration optimization for ^{209}Bi in AcAc medium (0.1%, v/v), UV irradiation time: 120 s, Co^{2+}(90 mg/L); (c)the media concentration optimization for ^{209}Bi, UV irradiation time: 120 s; Fe^{3+}(7 mg/L), Co^{2+}(90 mg/L); (d) the UV irradiation time optimization for ^{209}Bi in AcAc (0.05%, v/v) media, Fe^{3+}(7 mg/L), Co^{2+}(90 mg/L).

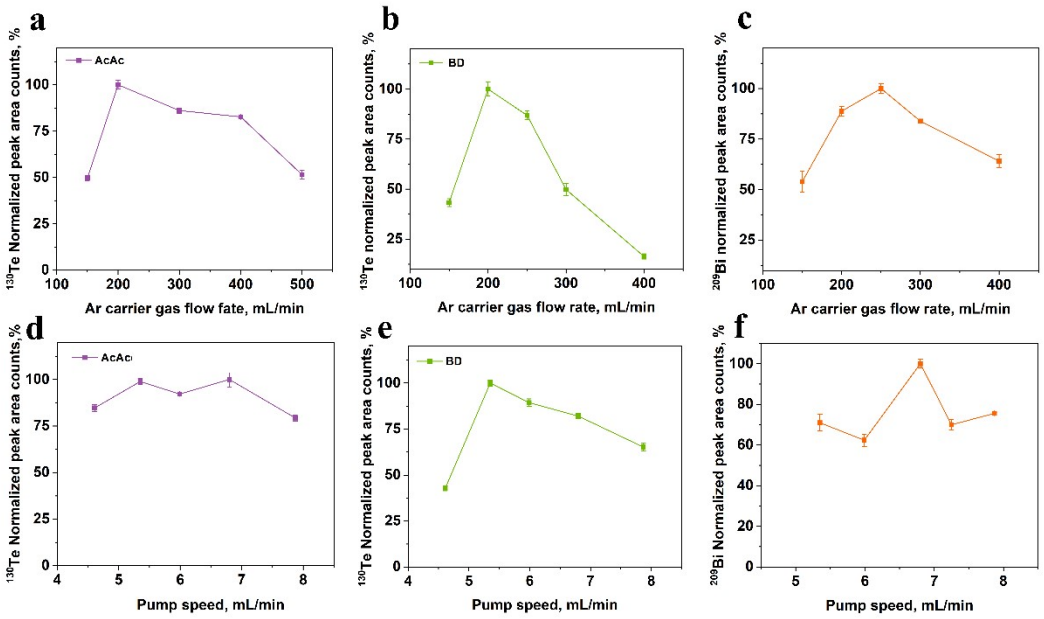

Fig. S6. the carrier gas flow rate and pump speed optimization for different elements in various media. (a-c) Ar carrier gas flow rate optimization, (d-f) pump speed optimization

Optimization of the carrier gas flow rate is essential. The impact of gas flow rate on PVG was studied in a range from 150 to 500 mL/min for Te in AcAc medium, 150 to 400 mL /min for Te in BD medium and 150 to 400 mL/min for Bi in AcAc medium. The optimal carrier gas flow rate in both of mediums was 200 mL/min for Te detection (Figure S6a, b) and 250 mL/min for Bi detection (Figure S6c). Finally, the optimized pump speed was 6.80 mL/min for Te in AcAc medium (Figure S6d), 5.35 mL/min in BD medium (Figure S6e) and a pump speed of 6.80 mL/min, which yielded the maximal ^{209}Bi peak area (Figure S6f).

Interference study

Table S1. Effects of Co-Existing Ions on Measurement of 10 µg/L Te (BD), (n=3)

Interfering ion	Interfering ions concentration (mg/L)	Recovery (%)
Na^{+}	20	91 ± 1
K^{+}	20	93 ± 2
Ca^{2+}	20	56 ± 1
Mg^{2+}	20	70 ± 3
Mn^{2+}	10, 20, 50	27 ± 2, 11 ± 0.4, 42 ± 3
Zn^{2+}	10, 20, 50	73 ± 3, 76 ± 2, 70 ± 2
Ni^{2+}	1, 5, 10	84 ± 3, 87 ± 2, 72 ± 1
Cu^{2+}	0.02, 0.2, 0.2[a]	62 ± 1, 40 ± 2, 46 ± 0.5
As^{3+}	1, 2	28 ± 1, 19 ± 0.8
NO_3^{-}	10, 20, 50	93 ± 2, 86 ± 1, 71 ± 4
SO_4^{2-}	10, 50	52 ± 1, 7 ± 1
CH_3COO^{-}	100	41 ± 2

[a] Recovery of Te with 20 mg/L DDTC.

Table S2. Effects of Co-Existing Ions on Measurement of 10 µg/L Te (AcAc), (n=3)

Interfering ion	Interfering ions concentration (mg/L)	Recovery (%)
Na^+	20	104 ± 2
K^+	20	104 ± 2
Ca^{2+}	20	80 ± 3
Mg^{2+}	20	101 ± 2
Mn^{2+}	10, 20, 50	90 ± 3, 89 ± 3, 87 ± 2
Zn^{2+}	10, 20, 50	96 ± 4, 96 ± 2, 98 ± 2
Ni^{2+}	1, 5, 10	103 ± 3. 94 ± 2, 93 ± 2
Cu^{2+}	0.02, 0.2, 0.2[a]	85± 3, 24 ± 3, 100 ± 3
As^{3+}	1, 2	109 ± 6, 113 ± 3
NO_3^-	10, 20, 50	108 ± 2, 90 ± 0.5, 81 ± 1
SO_4^{2-}	10, 50	105 ± 1, 105 ± 4
CH_3COO^-	100	96 ± 3

[a] Recovery of Te with 20 mg/L DDTC

Table S3. Effects of Co-Existing Ions on Measurement of 0.1 µg/L Bi (AcAc), (n=3)

Interfering ion	Interfering ions concentration (mg/L)	Recovery (%)
Na^+	1	105 ± 1
K^+	1	104 ± 2
Ca^{2+}	1	107 ± 2
Mg^{2+}	1	89 ± 1
Mn^{2+}	1	103 ± 2
Zn^{2+}	1	99 ± 4
Ni^{2+}	1	105 ± 3
Cu^{2+}	0.02	72 ± 1
As^{3+}	0.02	92 ± 1
Sb	0.02	88 ± 5
NO_3^-	1	103 ± 7
SO_4^{2-}	0.2	81 ± 2
CH_3COO^-	1	105 ± 3

In AcAc medium (Table S1), the effects from 20 mg/L Na^+, K^+ and Mg^{2+}, 50 mg/L Zn^{2+}, SO_4^{2-}, 10 mg/L Ni^{2+} and 100 mg/L CH_3COO^- on determination of 10 µg/L Te were negligible. Additionally, 20 mg/L Ca^{2+}, 50 mg/L Mn^{2+} and No_3^- and 2 mg/L As had reasonable impact on it. By contrast, these same ions had more obvious and negative impact on the determination of 10 µg/L Te in BD medium than AcAc medium with exception of Na^+ and K^+(Table S2). For the measurement of Bi (0.1 µg/L), the interference from most of ions was not obvious (Table S3). To be specific, 1 mg/L Na^+, K^+, Ca^{2+}, Mn^{2+}, Zn^{2+}, Ni^{2+}, NO_3^-, CH_3COO^- and 0.02 mg/L As^{3+} had negligible interference on the determination of 0.1 µg/L Bi. Furthermore, 1 mg/L Mg^{2+}, 0.2 mg/L SO_4^{2-} and 0.02 mg/L Sb had slight impact on it. On the contrary, Cu^{2+} exhibited a severe negative impact on determination of Te and Bi.

Table S4. Comparison of reagents consumption and limit of detection (LOD)

Element	Reagents and concentration	Instrument	LOD (μg/L)	ref
Te	AA (5 M) + FA (3.5 M)	ICP-MS	0.0013	1
Te	AA (20%) + FA (2%)	ICP-MS	0.001	2
Te	AA (20%) + FA (9%)	ICP-MS	0.0029	3
Te	AA (15%) + FA (10 %)	AFS	0.08	4
Te	AA (20%) + FA (5%)	AFS	0.6	5
Te	BD (0.09%)	ICP-MS	0.1	**this work**
Te	AcAc (0.1%)	ICP-MS	0.07	**this work**
Bi	AA (20%) + FA (5%)	ICP-MS	0.0003	6
Bi	AA (30%) + FA (10%)	ICP-MS	0.0003	7
Bi	AA (30%) + FA (10 %)	ICP-MS	0.0003	8
Bi	AcAc (0.05%)	ICP-MS	0.001	**this work**

Compared with the traditional low molecular weight organic acids (LMWOAs) PVG system, the consumption of reagent in diketone system is hundreds of times lower than LMWOAs system (Table. S4). In other words, diketones media could significantly alleviate the negative impacts of LMWOAs media, including the extremely acidic environment, sample contamination and environmental hazards. Although the diketone system shows limited performance in terms of LOD, this is reasonable for the novel PVG media as the research is still in the initial stage.

Table S5. The analytical results of Te and Bi in water samples by pneumatic nebulization inlet system (n=3)

Element	Water sample	Spiked (μg/L)	Found (μg/L)	Recovery (%)
Te	Nongfu Spring	0	0.0571 ± 0.003	\
		2.00	2.06 ± 0.007	100 ± 0.4
Te	Yan Lake	0	0.361 ± 0.007	\
		2.00	2.21 ± 0.02	92.3 ± 0.8
Bi	Nongfu Spring	0	N.D.	\
		0.0300	0.0291 ± 0.0004	97.0 ± 1.3
Bi	FANNY	0	N.D..	\
		0.0300	0.0285 ± 0.0004	95.0 ± 1.5

N.D.: not detected.

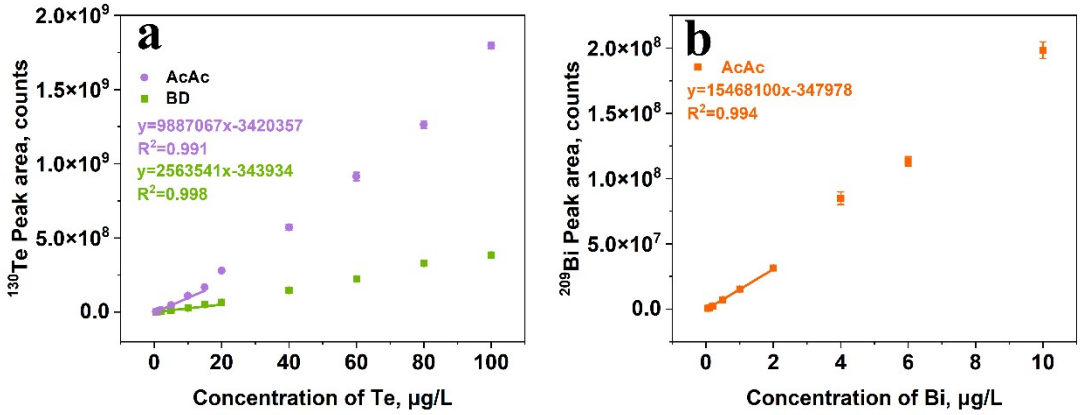

Fig. S7. The wide range calibration curves for Te and Bi. (a) Ranging from 0.5 to 100 μg/L. (b), Ranging from 0.05 to10 μg/L.

Although the calibration curves showcased excellent linear coefficients in a narrow range (0.5-10 μg/L for Te in AcAc and BD media and 0.01-1 μg/L for Bi in AcAc medium), the piece-wise linearity was observed unexpectedly. Specifically, the linear range for Te quantification was 0.5-15 μg/L in AcAc medium and 0.5-20 μg/L in BD medium (Fig. S7a). As for the detection of Bi (Fig. S7b), the linear range ran from 0.05 to 2 μg/L. We could not clarify this weird phenomenon, but we reckon that it is associated with the nanoparticles formation, because the similar phenomenon has been reported in previous study where nanoparticles were detected during chemical vapor generation (CVG).[9]

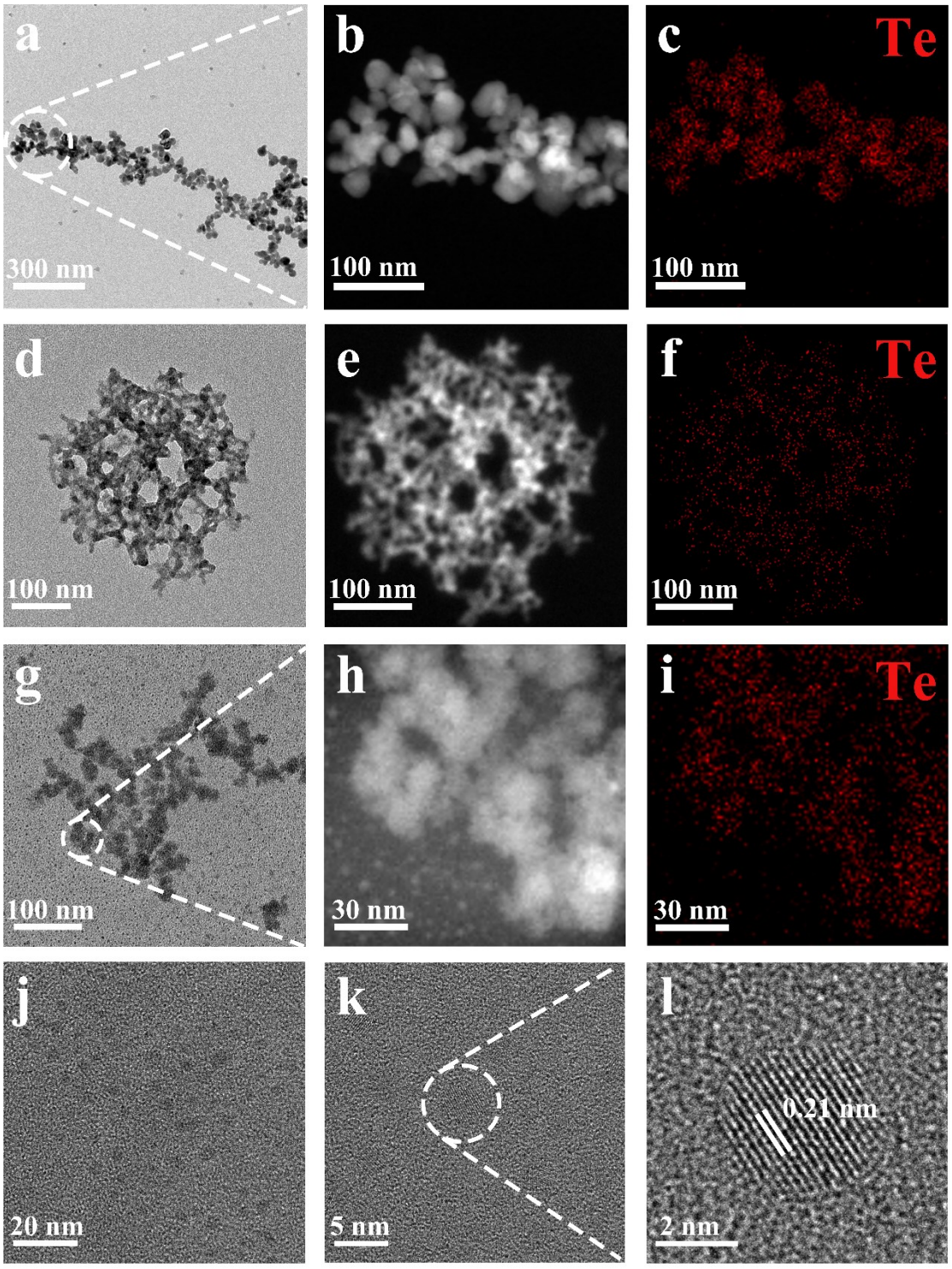

Fig. S8. TEM image of Te nanoparticles. (a-c) the Te nanoparticles in the liquid phase in BD medium, (d-f) the Te nanoparticles in the gaseous phase in BD medium, (g-i) the Te nanoparticles in the liquid phase in AcAc medium, (j-l) the Te nanoparticles in the gaseous phase in AcAc medium. Te concentration: 50 mg/L; AcAc concentration: 0.1% (v/v); BD concentration: 0.09% (v/v); 0.5 mg/L Fe^{2+} for BD media; 80 mg/L $Co^{2+}$for AcAc medium; UV irradiation time: 120 s.

In BD media, ions were reduced to nanoparticles in the liquid phase under UV irradiation (Fig. S8a, 8b). Energy-dispersive spectroscopy (EDS) confirmed that these nanoparticles were composed of Te (Fig. S8c). Subsequently, the Te nanoparticles in the liquid phase were separated and transferred into the gaseous phase using a gas-liquid separator (Fig. S8d, 8e, 8f). Similarly, in AcAc media, Te ions were reduced into nanoparticles (Fig S8g, 8h, 8i). However, the nanoparticles were so tiny and dispersive (Fig. S8j, 8k) that EDS could not be utilized to identify them. Fortunately, high-resolution transmission electron microscopy (HRTEM) revealed lattice spacings of 0.21 nm, confirming their composition as Te nanoparticles (Fig. S8l).

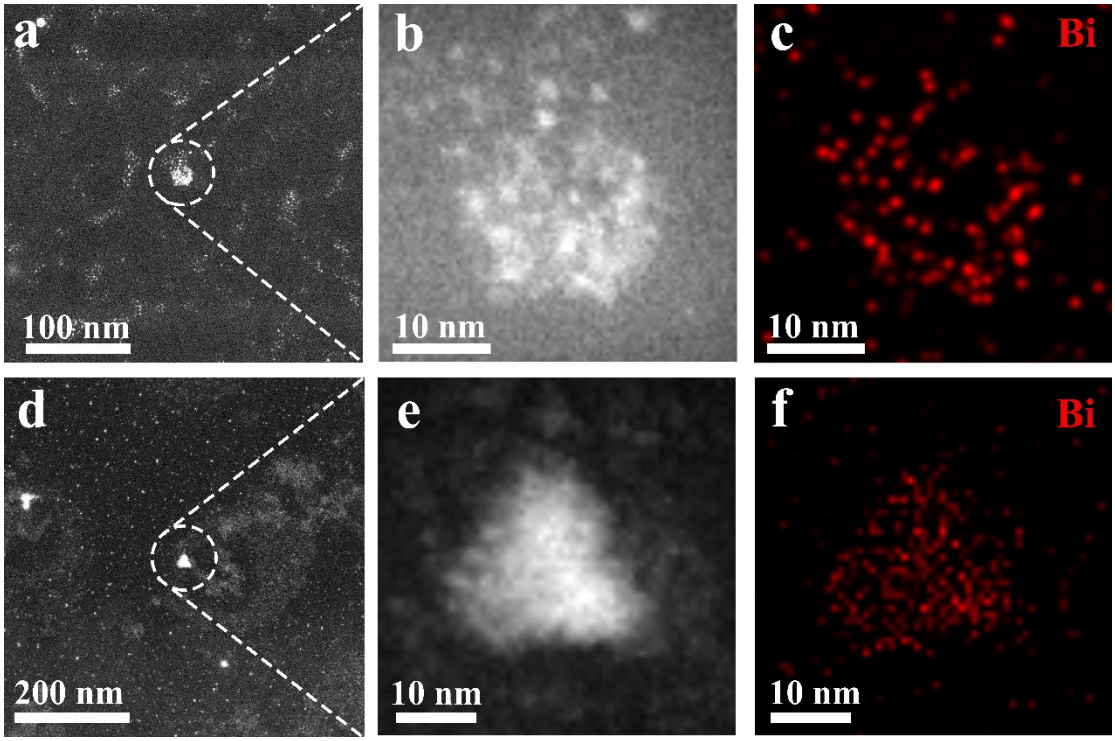

Fig. S9. TEM image of Bi nanoparticles. (a-c) the Bi nanoparticles in the liquid phase in AcAc medium, (d-f) the Bi nanoparticles in the gaseous phase in AcAc medium. Bi concentration: 20 mg/L; AcAc concentration: 0.05% (v/v); 7 mg/L Fe^{3+} and 90 mg/L Co^{2+} for AcAc medium; UV irradiation time: 150 s.

Following the same procedure, Bi nanoparticles formed by reduction in AcAc media under UV irradiation were identified. Utilizing TEM and EDS, we confirmed that Bi ions were reduced into nanoparticles (Fig. S9a, 9b, 9c) and transferred into gaseous phase (Fig. S9d, 9e, 9f) by gas-liquid separator.

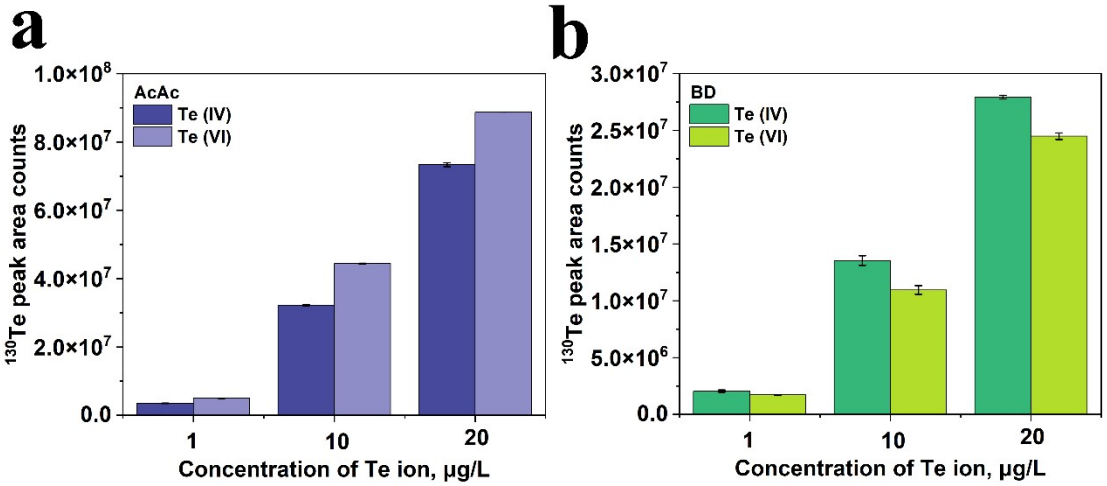

Fig. S10. Difference in the peak areas for Te(IV) and Te(VI) under the same experiment conditions. (a) Co^{2+}, 80 mg/L; UV irradiation time, 120 s; and AcAc, 0.1% (v/v); and (b) Fe^{2+}, 0.5 mg/L; UV irradiation time, 60 s; and BD, 0.09% (v/v).

The results shown in Fig. S10 indicate that the PVG responses of Te exhibit distinct behaviors depending on both the oxidation state of Te and the diketone medium employed. For Te(IV), comparable peak area responses are observed in AcAc and BD media under the conditions used in this experiment. For Te(VI), higher peak area responses are consistently observed in AcAc compared to BD. This trend is reasonable considering the higher reduction potential of Te(VI) and the more favorable photochemical reduction environment provided by AcAc. In contrast, the lower responses observed for Te(IV) in BD may be attributed to less efficient photochemical reduction pathways in this medium, which has also been reported previously for related systems. In summary, given the different signal responses of Te in various valence states, a pre-reduction step is required for total Te detection when using diketone media.

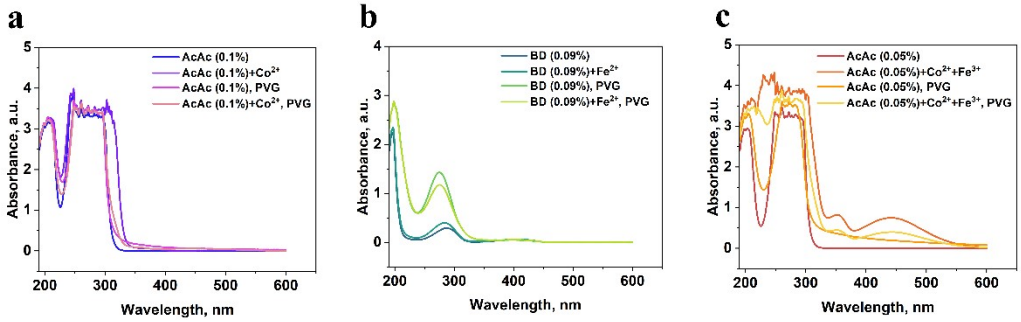

Fig. S11. The UV-vis spectra of the diketone media. (a) AcAc, 0.1% (v/v); Co^{2+}, 80 mg/L; and UV irradiation time, 120 s; (b) BD, 0.09% (v/v); Fe^{2+}, 0.5 mg/L; and UV irradiation time, 60 s; and (c) AcAc, 0.05% (v/v); Co^{2+}, 90 mg/L; Fe^{3+}, 7 mg/L; and UV irradiation time, 150 s. PVG means after UV irradiation.

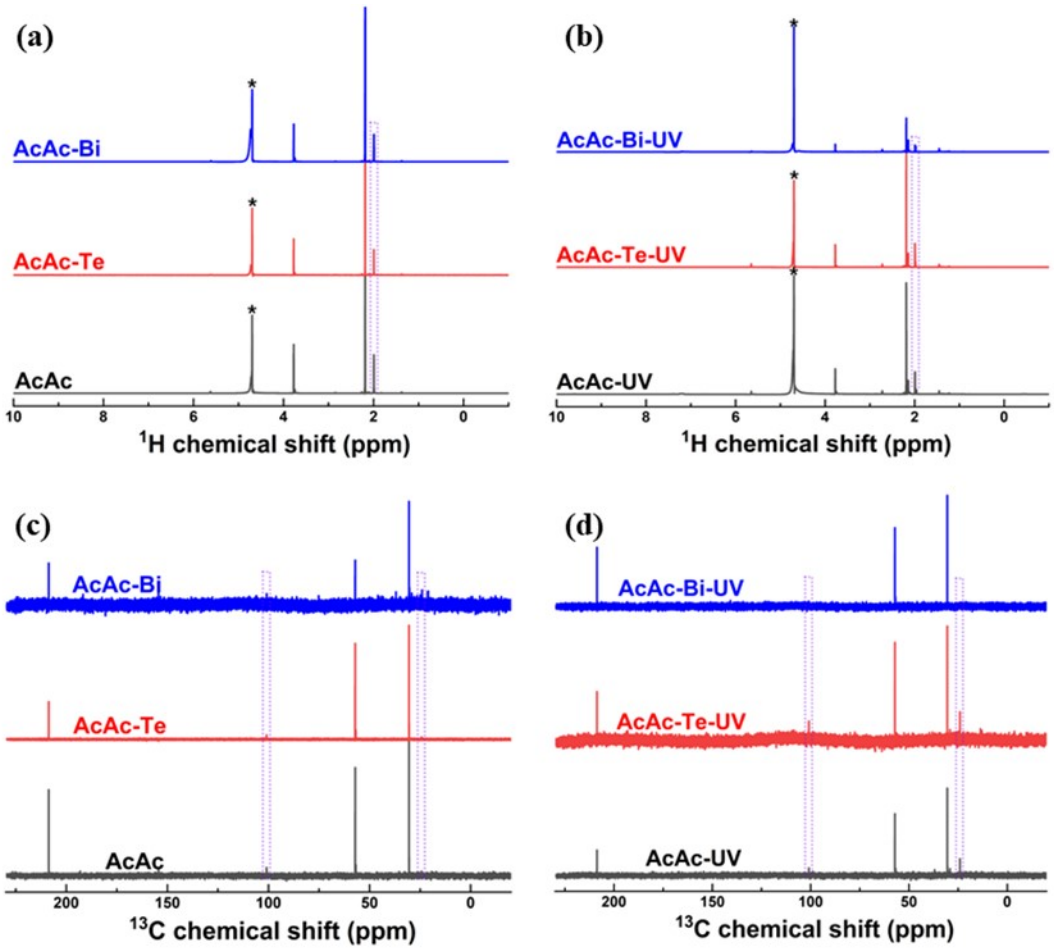

Fig. S12 ^{1}H-NMR spectra of the AcAc, AcAc-Te and AcAc-Bi systems before (a) and after (b) the UV irradiation. ^{13}C-NMR spectra of the AcAc, AcAc-Te and AcAc-Bi systems before (c) and after (d) the UV irradiation. The asterisks indicate the solvent peak of H_2O. Experimental condition: Te and Bi, both1 μg/L; AcAc and BD, both 0.6%, v/v; and UV irradiation time, 120 s and 150 s for Te and Bi, respectively.

Besides the direct reduction of Te and Bi by radicals, the diketone-Te or diketone-Bi complexations also played an important role in the reduction of Te and Bi. Consequently, the NMR techniques were for the first time employed to investigate the acetylacetone AcAc-Te and AcAc-Bi complexation systems during the photolysis procedure. As shown in Figure S12a and b, the AcAc exhibits keto-enol tautomerization in a mixed H_2O/D_2O solvent before and after UV irradiations, which is verified by the resonance at 2.04 ppm assigned to the hydrogen of the methyl attached to the olefinic carbon (highlighted by the purple box). Intriguingly, it was found that there was little influence on keto-enol tautomerization for the AcAc-Te system after UV irradiations. However, it is demonstrated that the keto-enol tautomerization was significantly suppressed attributing to the decreased intensity of the peak at 2.04 ppm for the AcAc-

Bi system after UV irradiations (highlighted by the purple box in Figure S12b). What's more, it is illustrated that the ^{13}C-NMR peaks at 100.5 ppm and 24.8 ppm assigned to the olefinic carbon and the methyl carbon attached to it respectively, were highly distinct for the AcAc-Te system after UV irradiations. On the other hand, the ^{13}C-NMR signals of the corresponding carbons discussed above could be barely detectable for the AcAc-Bi system after UV irradiations (highlighted by the purple box in Figure S12c and d). Based on the above analysis, it is rational to speculate that the AcAc-Te complex exists predominantly in the enol form, while the complex of AcAc-Bi exists mainly in the ketone form.

Reference

1. E. Jeníková, E. Nováková, J. Hraníček and S. Musil, *Anal. Chim. Acta*, 2022, **1201**, 339634.
2. H. He, X. Peng, Y. Yu, Z. Shi, M. Xu, S. Ni and Y. Gao, *Anal. Chem.*, 2018, **90**, 5737-5743.
3. L. Dong, H. Chen, Y. Ning, Y. He, Y. Yu and Y. Gao, *Anal. Chem.*, 2022, **94**, 4770-4778.
4. Y. Lu, C. Li, Y. Tian, J. Hu and X. Hou, *Anal. Chim. Acta*, 2023, **1247**, 340859.
5. W. Zeng, J. Hu, H. Chen, Z. Zou, X. Hou and X. Jiang, *J. Anal. At. Spectrom.*, 2020, **35**, 1405-1411.
6. Y. Yu, Y. Jia, Z. Shi, Y. Chen, S. Ni, R. Wang, Y. Tang and Y. Gao, *Anal. Chem.*, 2018, **90**, 13557-13563.
7. Y. Jia, Q. Mou, Y. Yu, Z. Shi, Y. Huang, S. Ni, R. Wang and Y. Gao, *Anal. Chem.*, 2019, **91**, 5217-5224.
8. Y. Yu, Q. Zhao, H. Bao, Q. Mou, Z. Shi, Y. Chen and Y. Gao, *Geostand. Geoanal. Res.*, 2020, **44**, 617-627.
9. Y. Zhen, T. Lin, H. Chen, J. Hu and X. Hou, *Anal. Chem.*, 2022, **94**, 15176-15182.
10. W. Huang, Y. Yu, L. Dong, X. Deng, X. Zhao, L. Liu and Y. Gao, *J. Anal. At. Spectrom.*, 2026, **41**, 363-371.